# Pressure-induced transition to the collapsed tetragonal phase in $BaCr_2As_2$

P. G. Naumov,[1,2] K. Filsinger,[1] O. I. Barkalov,[1,3] G. H. Fecher,[1] S. A. Medvedev,[1,*] and C. Felser[1]

[1]*Max Planck Institute for Chemical Physics of Solids, Nöthnitzer Straße 40, 01187 Dresden, Germany*

[2]*Shubnikov Institute of Crystallography of Federal Scientific Research Centre "Crystallography and Photonics" of Russian Academy of Sciences, Leninskii prospekt 59, Moscow 119333, Russia*

[3]*Institute of Solid State Physics, Russian Academy of Sciences, Academician Ossipyan strasse 2, Chernogolovka, Moscow District 142432, Russia*

(Received 7 February 2017; published 7 April 2017)

The structural and electronic properties of $BaCr_2As_2$, which is isostructural to the 122 iron arsenide superconductors, are studied at high pressures using synchrotron x-ray powder diffraction, electrical resistivity measurements, and first-principles calculations. At a pressure of about 18.5 GPa, an isostructural phase transition to a collapsed tetragonal phase is observed, similar to that in $BaFe_2As_2$. In both phases, $BaCr_2As_2$ is a normal metal. Electronic structure calculations suggest a metallic and antiferromagnetic ground state with $G$-type magnetic order for the collapsed tetragonal phase.

DOI: 10.1103/PhysRevB.95.144106

## I. INTRODUCTION

The discovery of iron-based superconductors in 2008 [1] has sparked a great deal of research aimed at understanding their properties and underlying physics. A variety of superconducting families have been identified, all of which share a common structural unit, namely, $Fe_2As_2$ or $Fe_2Se_2$ layers that are responsible for carrying superconductivity. Among these new superconductors, the so-called "122" compounds, which are ternary iron pnictides $AFe_2As_2$ (where $A$ represents alkaline-earth, rare-earth, or alkali metals) having $ThCr_2Si_2$-type crystal structures, are the most studied systems due to readily available high-quality single crystals with different doping levels.

In particular, intensive experimental and theoretical studies have considered the interplay of the structural, magnetic, and superconducting properties of the prototype system $BaFe_2As_2$, which undergoes a spin-density wave transition at $T_N = 132$ K concomitant with an orthorhombic structural distortion of the tetragonal $ThCr_2Si_2$-type structure [2]. Below $T_N$, $BaFe_2As_2$ is magnetically ordered with an antiferromagnetic stripe order of Fe moments aligned along the $a$ axis of the low-temperature orthorhombic crystal structure [3]. The spin-density wave (SDW) transition can be suppressed by doping with holes via chemical substitution of Ba (e.g., K for Ba) [4], or electrons via Fe substitution (Co for Fe) [5], or application of high pressure [6], resulting in the appearance of superconductivity. On the other hand, hole doping on the Fe site (substitution of Mn [7] or Cr [8] for Fe) does not lead to the appearance of superconductivity.

High pressure has been used as a method for tuning the ground state of a system without introducing a disordereffect, especially in studies of the relationship between the structure, magnetic properties, and superconductivity in Fe-based superconductors [9,10]. Because most Fe-based superconductors have a layered structure, the effect of pressure on the interaction between the layers is particularly important. Extensive experimental studies have shown a common structural trend for $AFe_2As_2$ compounds under pressure, namely, an isostructural transition from the tetragonal (T) structure to the so-called collapsed tetragonal (cT) structure. This isostructural transition is accompanied by negative compressibility of the tetragonal axis $a$, while both the $c$ and $c/a$ ratio decrease rapidly at pressures below the transition pressure ($P_c$) and decrease much more slowly above $P_c$ [11–16]. First-principles calculations reveal surprisingly strong interactions between the arsenic ions in iron pnictides $AFe_2As_2$, the strength of which is controlled by the Fe spin state: Reducing the Fe magnetic moment under applied pressure weakens the Fe-As bonding, and in turn, increases interlayer As-As interactions, causing a giant reduction in the $c$-axis length [17].

The pressure-induced isostructural transition to the cT phase is a common effect for compounds structurally related to $AFe_2As_2$, such as ternary europium phosphides $EuT_2P_2$ ($T$ indicates a transition metal) with the $ThCr_2Si_2$ structure in which the transition-metal element essentially determines the nature of this phase transition [18]. In this context, comparing the structural response of $BaFe_2As_2$ under pressure with that of analogous compounds with the same $ThCr_2Si_2$ structure but with a different transition element on the Fe site may be useful. An interesting candidate is $BaCr_2As_2$, which is structurally analogous to $BaFe_2As_2$ but has a different magnetic structure and bonding properties. While $BaFe_2As_2$ possesses an antiferromagnetic stripe order with only modest hybridization between the Fe $d$ and As $p$ states, theoretical calculations [19] for $BaCr_2As_2$ predicted an antiferromagnetic $G$-type checkerboard ordering (recently confirmed experimentally by neutron diffraction experiments [20]) with strong spin-dependent Cr $d$-As $p$ hybridization. Motivated by this combination of the similarity and differences in the crystalline and magnetic structures between $BaFe_2As_2$ and $BaCr_2As_2$, we have performed an experimental and theoretical study of the structural and electronic properties of $BaCr_2As_2$ under high pressure.

## II. EXPERIMENTAL AND COMPUTATIONAL DETAILS

Polycrystalline $BaCr_2As_2$ was synthesized by a prereaction of elemental Cr and As to CrAs, which was followed by a subsequent addition of Ba. Single crystals were grown from the resulting powder using the Bridgman method. To confirm the structure, powder and single-crystal x-ray diffraction (XRD) was performed on a Huber 670 Guinier camera

*Corresponding author: medvedie@cpfs.mpg.de

 

using Cu $K\alpha$ radiation ($\lambda = 1.540\,56$ Å). The microstructure was investigated using a FEI Titan 80-300 high-resolution transmission electron microscope (HRTEM). The composition was confirmed by inductively coupled plasma optical emission spectroscopy (ICP-OES) and energy dispersive x-ray spectroscopy (EDX). The average composition of the sample was $Ba_{1.03(4)}Cr_{2.01(5)}As_{2.03(5)}$. Further details on the synthesis and characterization of the sample are reported elsewhere [20].

For high-pressure generation, a diamond anvil cell (DAC) equipped with diamond anvils with 500-μm culets was used. The pressure was determined using the shift of the fluorescence line of ruby. All sample-loading procedures were performed in an Ar glove box with $O_2$ and $H_2O$ contents below 0.5 ppm.

For synchrotron XRD studies, a powdered sample of $BaCr_2As_2$ was loaded in the central hole (~150-μm diameter) of a tungsten gasket preindented to a thickness of ~40 $\mu$m, using silicone oil as a pressure transmitting medium. The angle-dispersive XRD measurements were performed at the ID-27 beamline at the European Synchrotron Radiation Facility (ESRF, Grenoble, France). The wavelength of the x rays (0.3738 Å) was selected using a Si(111) monochromator. The sample-to-image plate (MAR345) detector distance was refined using the diffraction data of Si. The two-dimensional powder images were integrated using the program FIT2D to yield the intensity versus $2\theta$ plot.

For electrical resistivity measurements, a $BaCr_2As_2$ single crystal of a suitable size was placed into the central hole of a tungsten gasket with an insulating cubic BN/epoxy layer. Electrical resistivity at different pressures in the temperature range 1.5–300 K was measured with dc current using the Van der Pauw technique with Pt electrodes attached to the sample.

The electronic structure of $BaCr_2As_2$ was calculated in the local spin-density approximation (LSDA). The self-consistent band structure calculations were performed using the full-potential linearized augmented-plane wave (FLAPW) method as implemented in WIEN2K [21–23]. The spin-orbit (SO) interaction is treated in FLAPW as a perturbation using the second variational method. All calculations were performed using the generalized gradient approximation (GGA) by Perdew, Burke, and Ernzerhof (PBE) [24]. The integration in wien2k was based on a $(20 \times 20 \times 20)$ $k$ mesh with the number of plane waves restricted to $R_{MT}k_{max} = 7$. The potential was expanded in spherical harmonics up to $l = 6$ and wave functions up to $l = 10$. The convergence criteria were set to $10^{-5}$ and $10^{-3}$ for the energy and charge convergence, respectively. The electronic structure was calculated for $Cu_2TlSe_2$ ($tI10$, $I4/mmm$, 139). Further, a $G$-type antiferromagnetic order was assumed, and the lattice was set up with reduced symmetry in $I\bar{4}m2$ (119) with Ba on $2a$ and As on $4e$. The Cr atoms are located on split $2c$ and $2d$ sites to allow for antiparallel orientations of their magnetization. This space group is concerned with the atomic positions, while the final magnetic symmetry depends on the direction of the quantization axis and is described by a Shubnikov color group. Further details of the electronic structure calculations are presented elsewhere [20].

## III. RESULTS AND DISCUSSION

The x-ray diffraction pattern of powdered $BaCr_2As_2$ in the DAC at 1 GPa (Fig. 1) can be unambiguously indexed with the $ThCr_2Si_2$ ($I4/mmm$) structure. The lattice parameters are in good agreement with the ambient-pressure data. The temperature dependence of the resistivity at 1.3 GPa (Fig. 2) shows metallicklike behavior in agreement with the published ambient-pressure data [19]; however, an upturn in the resistivity is observed at temperatures below 50 K, similar to that observed in $BaFe_{1.95}Cr_{0.05}As$ [25].

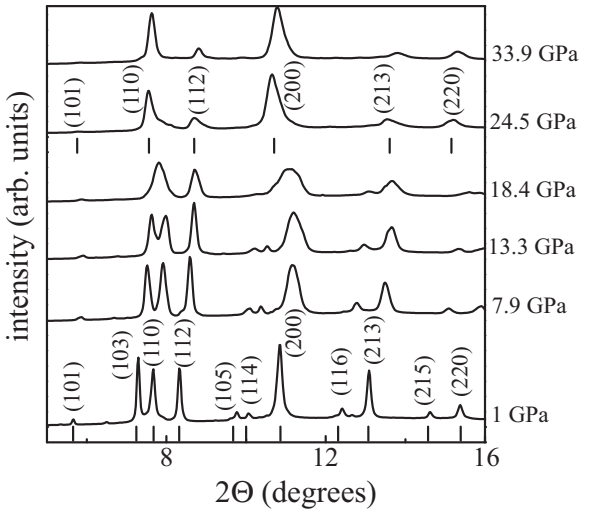


FIG. 1. X-ray diffraction patterns of $BaCr_2As_2$ at different pressures. All patterns can be indexed with the tetragonal $I4/mmm$ structure, as indicated by the indices above the calculated reflection positions and denoted by tick marks under the patterns.

The XRD patterns of $BaCr_2As_2$ collected at pressures up to 34 GPa are shown in Fig. 1. All patterns up to the highest pressure can be properly indexed with the tetragonal $ThCr_2Si_2$-type structure. However, the pressure evolution of the patterns shows peculiar behavior.

At pressures below 15 GPa, all diffraction peaks shift towards higher diffraction angles due to the decrease of the lattice parameters with increasing pressure [Figs. 3(a) and 3(b)].

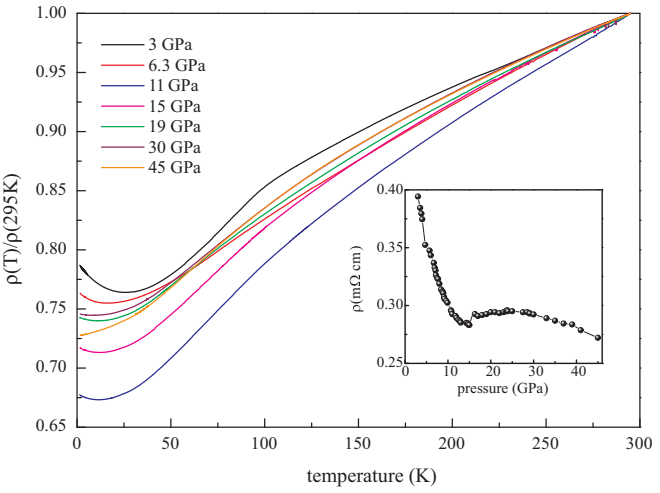


FIG. 2. Normalized temperature dependence of the electrical resistivity of $BaCr_2As_2$ at selected pressures. The inset shows the pressure dependence of the electrical resistivity at room temperature.

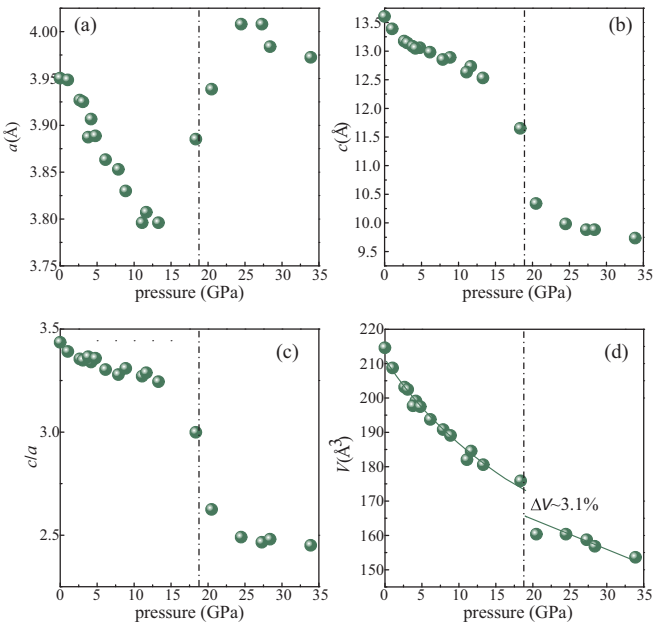


FIG. 3. Pressure dependence of the lattice parameters $a$ (a), $c$ (b), $c/a$ ratio (c), and unit cell volume $V$ (d). Vertical dash-dot lines on all panels indicate the pressure ($P_c$) of the tetragonal-to-collapsed-tetragonal phase transition. The solid line within the tetragonal phase in panel (d) is the fitting of the experimental data to the third-order Birch-Murnaghan equation of state.

The compressibility of the lattice is anisotropic, resulting in a gradual decrease of the $c/a$ ratio for pressures below 15 GPa [Fig. 3(c)]. Fitting the second-order Birch-Murnaghan equation of state to the measured pressure-volume data at pressures below 15 GPa [Fig. 3(d)] provides the bulk modulus value $B_0 = 63.1 \pm 3.8$ GPa (with a fixed pressure derivative of bulk modulus $B' = 4$), which is in good agreement with the corresponding values for tetragonal $ThCr_2Si_2$-type structures of pristine [13] and Cr-doped [25] $BaFe_2As_2$ and structurally related materials [16].

Above 15 GPa, the $2\theta$ positions of the (110) and (200) Bragg peaks related with the $a$ axis decrease as pressure increases, contrary to conventional lattice behavior under compression. This behavior indicates anomalous (negative) compressibility of the $a$ axis [Fig. 3(a)] accompanied with a sharp decrease in the $c$ axis [Fig. 3(b)] with the application of pressure. Such structural trends are observed in a number of compounds with tetragonal $ThCr_2Si_2$-type structures, and it is a manifestation of an isostructural phase transition from the tetragonal (T) to the collapsed tetragonal (cT) phase [18]. The pressure dependence of the lattice parameters $a$ and $c$, the $c/a$ ratio, and the unit cell volume of $BaCr_2As_2$ (Fig. 3) is very similar to that observed in $BaFe_2As_2$. Detailed structural studies of superconducting $BaFe_2As_2$ at high hydrostatic pressures revealed a first-order phase transition to the cT phase at 27 GPa [11]. Our XRD studies have been performed only at increasing pressure; thus hysteresis was not observed, and the pressure of the transition can only be estimated to occur at $P_c \approx 18.5$ GPa with a volume jump of $\approx 3.1\%$.

The transformation from the T to the cT phase is suggested to be a universal characteristic of $AFe_2As_2$ compounds [12,14,16] since experimental studies reveal this common structural trend under pressure in superconducting $AFe_2As_2$ with $A$ being a divalent (Ca [11,26], Ba [11,13], Sr [15], Eu [14,16]) or monovalent (Na [12]) metal. The pressure ($P_c$) of the transition to the cT phase depends on the size of the cation $A$ [14,16]. Interestingly, even though the tetragonal $G$-type antiferromagnetic $BaMn_2As_2$ undergoes an isostructural electronic phase transition at $\sim$5 GPa that is associated with metallization, this transition is clearly different from the T-cT transitions in the $AFe_2As_2$ family [27]. Our results reveal that the high-pressure structural behavior of $G$-type antiferromagnetic $BaCr_2As_2$ is quite similar to that of itinerant $BaFe_2As_2$. The antiferromagnetic $BaMn_2As_2$ thus represents a peculiar case that originates from strong Hund's coupling, the stability of the half-filled $d$ shell of the $Mn^{+2}$ ($d^5$) ion, and strong spin-dependent Mn-As hybridization [28,29]. The unit cell volume of $BaMn_2As_2$ is significantly larger than that of the rest of the materials in the $BaT_2As_2$ series indicating the high spin state of the Mn ion [29]. The isostructural transition at $\sim$5 GPa is apparently of electronic nature which might involve high-spin–low-spin transition, and the nature of this transition remains to be studied in detail [27]. Pressure studies of $BaMn_2As_2$ have been performed only up to 10 GPa, so far; however, the transition to the cT phase can also be expected but at pressures well above 20 GPa. The observation of this transition and changes of electronic transport properties associated with this transition would be of interest.

The electronical transport properties of $BaCr_2As_2$ remain qualitatively unchanged with the transition in the cT phase. At all tested pressures up to 45 GPa, $BaCr_2As_2$ shows metallic behavior (Fig. 2). At all pressures within the stability range of the tetragonal phase, no resistivity anomalies were observed due to magnetic ordering at temperatures below 300 K. Thus it might be supposed that the Néel temperature of tetragonal $BaCr_2As_2$ remains above room temperature with pressure increase up to the cT phase transition. The room-temperature resistivity of the sample gradually decreases in the tetragonal phase (inset in Fig. 2). At the transition to the cT phase, the room-temperature resistivity shows a discontinuous increase followed by a subsequent slight increase up to $\sim$25 GPa, which gradually decreases with a further pressure increase (inset in Fig. 2), reflecting the pressure behavior of lattice parameter $a$ [Fig. 3(a)] and thus the interatomic Cr-Cr distances. The resistivity upturn for temperatures below 50 K observed at low pressures is gradually suppressed as pressure increases. No signs of superconductivity have been observed with $T_c > 1.5$ K up to 45 GPa.

To obtain additional insight into the properties of the cT phase of $BaCr_2As_2$, the electronic structure calculations within the GGA approach have been performed using the experimentally determined lattice parameters. The quality of our high-pressure diffraction patterns obtained under quasi-hydrostatic conditions is not sufficient to perform full-profile Rietveld structural refinements. Therefore, the $z$ coordinate of the As atoms in both T and cT phases (Fig. 4) has been obtained by structural optimization via total energy calculations. These results reveal a rapid decrease of the interlayer As-As distances in the tetragonal phase (Fig. 4), accounting for the $c$-axis contraction with pressure increase. At the transition to the cT phase, the interlayer As-As distance abruptly decreases

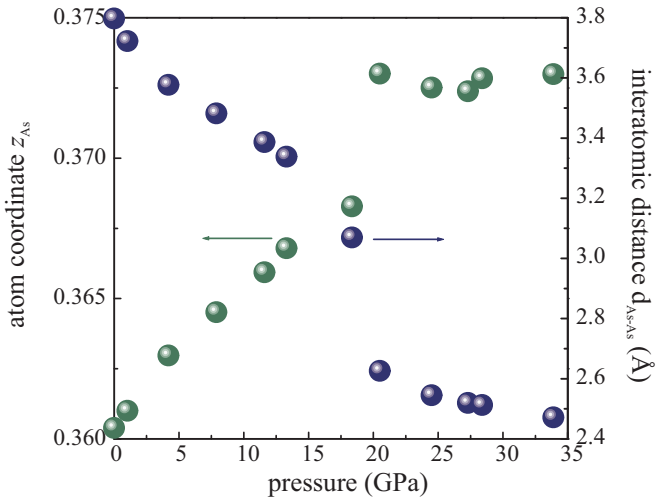


FIG. 4. Optimized $z$ parameter of the As atoms at the Wyckoff $4e$ position of the $I4/mmm$ structure (green symbols) and the interatomic interlayer As-As distance along the $c$ axis of $BaCr_2As_2$ (green symbols).

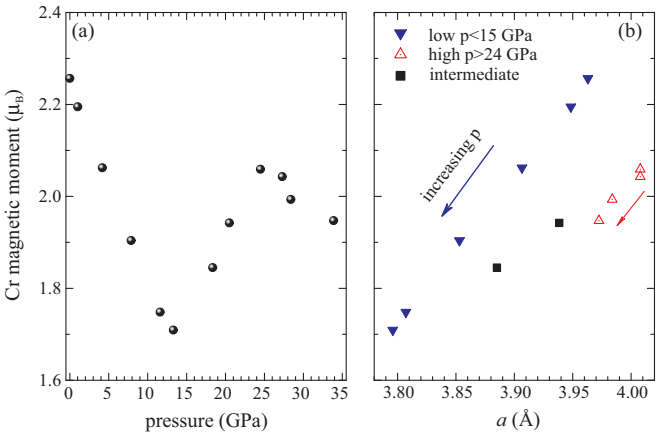


FIG. 5. Pressure (a) and lattice parameter dependence (b) of the Cr magnetic moments in $BaCr_2As_2$.

to ∼2.5 Å (which is in the range of a single As-As covalent bond distance ∼2.4 Å), indicating the possible formation of interlayer As-As bonds. The formation of single interlayer P-P bonds at the pressure-induced transition to the cT phase was established for structurally related ternary europium phosphides with the $ThCr_2Si_2$ structure [18]. Furthermore, the As-As hybridization and the abrupt decrease of the As-As distances to values very close to the As-As covalent bond distance in the cT phase under high pressure in $AFe_2As_2$ superconductors was theoretically predicted [17], and recent experimental studies of $NaFe_2As_2$ have shown the formation of As-As interlayer bonding in the cT phase [12].

Theoretical calculations for superconducting $AFe_2As_2$ reveal strong interactions between arsenic ions, the strength of which is controlled by the Fe spin state: Reducing the Fe magnetic moment weakens the Fe-As bonding, and in turn, increases As-As interactions [17]. Our results for $BaCr_2As_2$ reveal the same trend for Cr-based compounds. Under compression, the magnetic moment of Cr decreases [Fig. 5(a)], whereas the strength of the As-As interaction increases (Fig. 4). Furthermore, the results of our calculations show that the Cr magnetic moment does not vanish (although it is suppressed) after the transition to the cT phase; thus the cT phase of $BaCr_2As_2$ is magnetic. This behavior is similar to that of $NaFe_2As_2$ [12]. The dependence of the magnetic moment on pressure [Fig. 5(a)] shows complex behavior resembling the nonmonotonic behavior of the lattice parameter $a$ [Fig. 3(a)]. The strong coupling between the magnetic moment and structural parameters is even more evident from a more detailed analysis, distinguishing the low- and high-pressure regions [Fig. 5(b)]. The change in the magnetic moment still appears with the lattice parameter $a$ rather than other parameters. The magnetic moment increases with increasing $a$, that is, with increasing Cr-Cr distances.

The total energy calculations reveal that the $G$-type antiferromagnet is lowest in the complete pressure range up to 34 GPa. The energy differences for spin-nonpolarized (PM), as well as spin-polarized ferromagnetic (FM) or $G$-type antiferromagnetic (AFM), calculations are shown in Fig. 6. The volume of the cell and the $c/a$ ratio decrease drastically in the pressure range between 15 and 20 GPa. A sudden decrease in the volume appears with the observed discontinuity of the total energy. The temperature dependence of the electrical resistivity during cooling from room temperature to 1.5 K in the cT phase (Fig. 2) reveals no anomalies that can be attributed to magnetic ordering. Thus it might be supposed that the antiferromagnetic ordering temperature in the cT phase is above room temperature at least up to the highest pressures of 45 GPa.

Thus a transition from the antiferromagnetic state into another magnetic state can be excluded from the behavior of the total energy under pressure. It was further investigated whether the antiferromagnetic order changes its direction. Therefore, calculations were performed including the spin-orbit interaction with magnetization along different quantization axes, namely, [100], [110], [001] (Table I). Alignment along the $c$ axis has the lowest energy for the cases at 0 and 34 GPa, in other words, in both the T and cT phases. The anisotropy of energies between the $ab$ plane and the $c$ axis are considerably weaker for the high-pressure structure. The

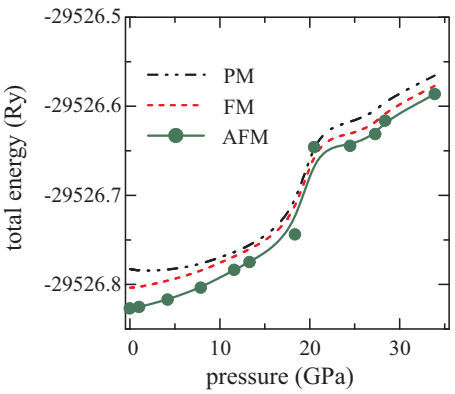


FIG. 6. Total energies for non-spin-polarized (PM), ferromagnetic (FM), and $G$-type antiferromagnetic (AFM) cases calculated using the experimental lattice parameters at various applied pressures.

TABLE I. Magnetic anisotropy of $BaCr_2As_2$. Tabulated are the magnetic symmetries, total energies, and spin moments $m_{Cr}$ at the Cr atoms, calculated at both ambient and high pressure for different directions of the quantization axis $\vec{B}$. Here, $\Delta E = E - E_{min}$, where $E_{min}$ is the lowest total energy at a given pressure, and $\Delta E$ is given in micro electron volts. The magnetic moments $m_{Cr}$ of the Cr atoms are given in multiples of the Bohr magneton $\mu_B$.

| | | | $P = 0$ | | $P = 34$ GPa | |
|---|---|---|---|---|---|---|
| $\vec{B}$ | Shubnikov group | | $\Delta E$ | $m_{Cr}$ | $\Delta E$ | $m_{Cr}$ |
| [100] | $Pm'mm$ | (47.251) | 429 | 2.395 | 16 | 2.039 |
| [110] | $Cm'mm$ | (65.483) | 410 | 2.396 | 28 | 2.038 |
| [001] | $P4'/m'm'm$ | (123.344) | 0 | 2.397 | 0 | 2.039 |

magnetic anisotropy between the two different directions in the $ab$ plane is small and of the same order in both cases, but changes sign between the low- and high-pressure phases.

Figure 7 compares the calculated band structures for $P = 0$ and 18 GPa. A strong shift of the bands is observed in the vicinity of the Fermi energy ($\varepsilon_F$) to lower energies. At 18 GPa, two bands touch $\varepsilon_F$ at the $\Gamma$ point. These bands have a minimum at $\Gamma$ in the $\overline{S_1\Gamma X}$ direction. In the $\overline{M\Gamma N}$ direction, the upper band exhibits a minimum, whereas the lower band has a maximum. Thus the lower band has a saddle-point-type Van Hove singularity. This particular band structure leads to a maximum in the density of states that appears at the Fermi energy. The result is instability of the tetragonal lattice that occurs for pressures of about 18 GPa, triggering the phase transition to the cT phase.

Finally, the question arises regading at what pressure the antiferromagnetic order would vanish. The result for the calculated magnetic moment is shown in Figure 8. First, an estimate is found using a hydrostatic model using the low-pressure structure and reducing only the volume with the applied pressure. That is, $a$ and $c$ are reduced with a constant $c/a$ ratio whereas position parameter $z$ for the As atoms is fixed at the value obtained from the structure relaxation at low pressures. The pressure is determined from the energy-volume relation using the Birch-Murnaghan equation of state. The

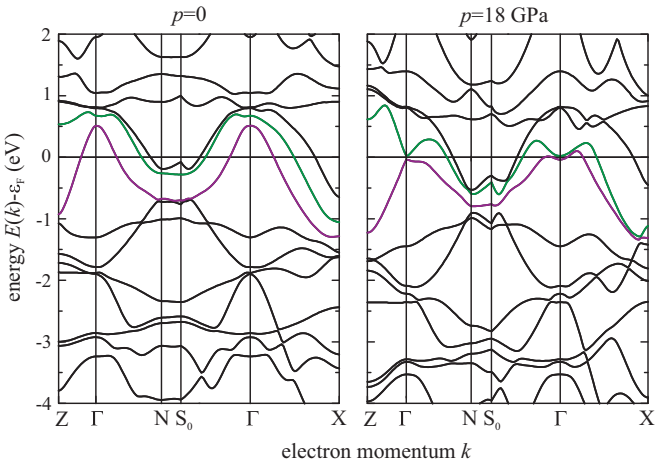


FIG. 7. Pressure dependence of the band structure of $BaCr_2As_2$.

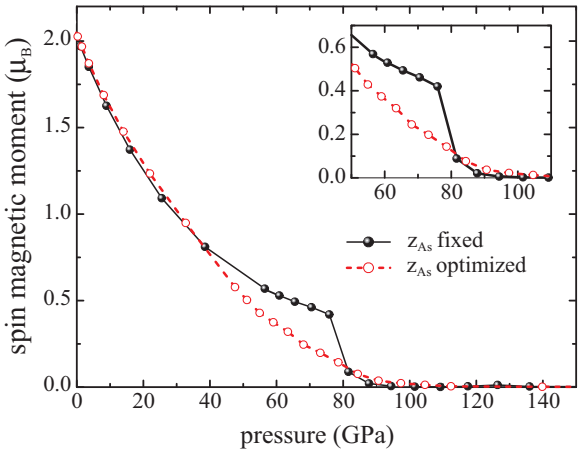


FIG. 8. Collapse of the magnetic moment at very high pressure. The calculation is performed for fixed and optimized $z$ position parameters of the As atoms.

internal pressure (internal force acting on the atom appears due to the dependence of energy on the positional parameter which is out of equilibrium if the atomic position is not relaxed) was neglected when the fixed position parameter $z$ for the As atoms is used. At this level of calculations, the magnetic moment of the Cr atoms decreases continuously with increasing pressure and collapses at about 80 GPa. To release the internal pressure, the position parameter $z$ was optimized at each volume. In that case, the magnetization decreases continuously until it vanishes. In both cases, with and without optimizing the $z$ parameter, the magnetic moment becomes zero at pressures above 100 GPa (see Fig. 8).

## IV. CONCLUSIONS

We have studied the effect of pressure on the structural and electronic properties of $BaCr_2As_2$, which is isostructural to the 122 iron arsenide superconductors. Synchrotron x-ray diffraction data show a phase transition from the tetragonal phase to the collapsed tetragonal phase at about 18.5 GPa. Both phases of $BaCr_2As_2$ are normal metals without any signs of superconductivity up to 45 GPa. Theoretical calculations reveal that the high-pressure collapsed tetragonal phase remains magnetic with $G$-type antiferromagnetic ordering. Electronic structure calculations indicate that a saddle-point-type Van Hove singularity at a pressure near the phase transition (of around 18 GPa) might result in instability of the lattice, triggering the phase transition to the cT phase.

## ACKNOWLEDGMENTS

This work was supported by the Deutsche Forschungsgemeinschaft within Priority Program No. 1458 by Grant No. ME 3652/1-2. We acknowledge the European Synchrotron Radiation Facility for granting the beam time, and we are grateful to Dr. M. Mezouar and Dr. G. Garbarino (ESRF) for assistance in using beamline ID27.

[1] Y. Kamihara, T. Watanabe, M. Hirano, and H. Hosono, J. Am. Chem. Soc. **130**, 3296 (2008).

[2] M. Rotter, M. Tegel, D. Johrendt, I. Schellenberg, W. Hermes, and R. Pöttgen, Phys. Rev. B **78**, 020503 (2008).

[3] Q. Huang, Y. Qiu, W. Bao, M. A. Green, J. W. Lynn, Y. C. Gasparovic, T. Wu, G. Wu, and X. H. Chen, Phys. Rev. Lett. **101**, 257003 (2008).

[4] M. Rotter, M. Tegel, and D. Johrendt, Phys. Rev. Lett. **101**107006 (2008).

[5] A. S. Sefat, R. Jin, M. A. McGuire, B. C. Sales, D. J. Singh, and D. Mandrus, Phys. Rev. Lett. **101**, 117004 (2008).

[6] P. L. Alireza, C. Y. T. Ko, J. Gillett, C. M. Petrone, J. M. Cole, G. G. Lonzarich, and S. E. Sebastian, J. Phys.: Condens. Matter **21**, 012208 (2009).

[7] D. Kasinathan, A. Ormeci, K. Koch, U. Burkhardt, W. Schnelle, A. Leithe-Jasper, and H. Rosner, New J. Phys. **11**, 025023 (2009).

[8] A. S. Sefat, D. J. Singh, L. H. VanBebber, Y. Mozharivskyj, M. A. McGuire, R. Jin, B. C. Sales, V. Keppens, and D. Mandrus, Phys. Rev. B **79**, 224524 (2009).

[9] L. Malavasi and S. Margadonna, Chem. Soc. Rev. **41**, 3897 (2012).

[10] A. S. Sefat, Rep. Prog. Phys. **74**, 124502 (2011).

[11] R. Mittal, S. K. Mishra, S. L. Chaplot, S. V. Ovsyannikov, E. Greenberg, D. M. Trots, L. Dubrovinsky, Y. Su, T. Brueckel, S. Matsuishi, H. Hosono, and G. Garbarino, Phys. Rev. B **83**, 054503 (2011).

[12] E. Stavrou, X.-J. Chen, A. R. Oganov, A. F. Wang, Y. J. Yan, X. G. Luo, X. H. Chen, and A. F. Goncharov, Sci. Rep. **5**, 9868 (2015).

[13] W. Uhoya, A. Stemshorn, G. Tsoi, Y. K. Vohra, A. S. Sefat, B. C. Sales, K. M. Hope, and S. T. Weir, Phys. Rev. B **82**, 144118 (2010).

[14] W. Uhoya, G. Tsoi, Y. K. Vohra, M. A. McGuire, A. S. Sefat, B. C. Sales, D. Mandrus, and S. T. Weir, J. Phys.: Condens. Matter **22**, 292202 (2010).

[15] W. O. Uhoya, J. M. Montgomery, G. M. Tsoi, Y. K. Vohra, M. A. McGuire, A. S. Sefat, B. C. Sales, and S. T. Weir, J. Phys.: Condens. Matter **23**, 122201 (2011).

[16] Z. Yu, L. Wang, L. Wang, H. Liu, J. Zhao, C. Li, S. Sinogeikin, W. Wu, J. Luo, N. Wang, K. Yang, Y. Zhao, and H.-K. Mao, Sci. Rep. **4**, 7172 (2014).

[17] T. Yildirim, Phys. Rev. Lett. **102**, 037003 (2009).

[18] C. Huhnt, W. Schlabitz, A. Wurth, A. Mewis, and M. Reehuis, Physica B **252**, 44 (1998).

[19] D. J. Singh, A. S. Sefat, M. A. McGuire, B. C. Sales, D. Mandrus, L. H. VanBebber, and V. Keppens, Phys. Rev. B **79**, 094429 (2009).

[20] K. A. Filsinger, W. Schnelle, P. Adler, G. H. Fecher, M. Reehuis, A. Hoser, J.-U. Hoffmann, P. Werner, M. Greenblatt, and C. Felser, arXiv:1701.03127.

[21] P. Blaha, K. Schwarz, P. Sorantin, and S. B. Trickey, Comput. Phys. Commun. **59**, 399 (1990).

[22] K. Schwarz and P. Blaha, Comput. Mater. Sci. **28**, 259 (2003).

[23] P. Blaha, K. Schwarz, G. K. H. Madsen, D. Kvasnicka, and J. Luitz, *WIEN2K, an Augmented Plane Wave + Local Orbitals Program for Calculating Crystal Properties*, revised ed. 14.2 (Karlheinz Schwarz, Technische Universitaet Wien, Wien, Austria, 2014).

[24] J. P. Perdew, K. Burke, and M. Ernzerhof, Phys. Rev. Lett. **77**, 3865 (1996).

[25] W. O. Uhoya, J. M. Montgomery, G. K. Samudrala, G. M. Tsoi, Y. K. Vohra, S. T. Weir, and A. S. Sefat, J. Phys. Conf. Ser. **377**, 012016 (2012).

[26] A. Kreyssig, M. A. Green, Y. Lee, G. D. Samolyuk, P. Zajdel, J. W. Lynn, S. L. Bud'ko, M. S. Torikachvili, N. Ni, S. Nandi, J. B. Leão, S. J. Poulton, D. N. Argyriou, B. N. Harmon, R. J. McQueeney, P. C. Canfield, and A. I. Goldman, Phys. Rev. B **78**, 184517 (2008).

[27] A. T. Satya, A. Mani, A. Arulraj, N. V. Chandra Shekar, K. Vinod, C. S. Sundar, and A. Bharathi, Phys. Rev. B **84**, 180515(R) (2011).

[28] J. An, A. S. Sefat, D. J. Singh, and M.-H. Du, Phys. Rev. B **79**, 075120 (2009).

[29] D. C. Johnston, Adv. Phys. **59**, 803 (2010).